Thermography – A Big Data Problem (Experiments)

Tian Xiao[1], Dr Henry Goh Kok Hin[2]

[1]H3 NUS-A*Star-NJC Science Research Student, National Junior College

[2]Institute of Materials Research and Engineering

Abstract

In this paper, two techniques of identifying the geometry of objects using Lock-in Thermography (LIT) are discussed. Identifying geometries can be applied into many areas, such as global scanning and detecting interior defects. LIT is a widely used non-destructive technique (NDT) where a periodic power input is applied onto the surface of an object and the response signals are captured and analysed. Thousands of data points are obtained from each sample for analysis. The main idea of both techniques is to link the thickness of each data point to the response signal. With the thickness and the coordinates of each data point, the 3-dimensional geometry of the whole object can be obtained. Evaluation of the techniques include both root-mean-square deviation (RMSD), a common quantitative standard statistical performance evaluation measure, and calculation of successful rate with a tolerance. The results show that the second technique performs better than the first. Moreover, when applying the techniques, stochastic gradient decent (SGD) can be used to generate the geometry during the measurement, which makes the techniques more applicable. However, limitations of SGD in this case are also discussed.

1. Introduction

Infrared thermography (IRT) is a technique based on detection of objects radiation in the infra-red range [1] that has applications in many different areas such as architecture [2], biology [3] and even geography [4]. As IRT applies only infra-red rays onto objects, it does not cause damage to the objects [5]. Hence, it is commonly used as a non-destructive testing (NDT) technique to detect defects in objects [6, 7, 8].

IRT is categorised into two types: passive thermography and active thermography [9]. Passive thermography measures the variation of temperature across the surface of objects or the natural temperature change of objects [10]. On the other hand, in the case of active thermography, an external heat source is used for excitation of the analysed objects. The excitation causes a temperature contrast connected with factors such as thermal properties differences or local heat sources concentration [11].

Lock-in Thermography (LIT) is one example of active thermography, which is about applying a periodic power input onto the surface of an object and analysing the resulting surface temperature [12]. Amplitude and phase of the response signal is analysed by different techniques. For example, the phase signal is found to be useful in highlighting defects or other anomalies when using different lock-in frequencies [13, 14]. However, it has not been found to have a direct correlation with physical properties of the object, such as its thickness, emissivity, etc [15].

There are attempts made to map the thickness of an object [16] or its coating [17] to the signal obtained from LIT. The aim of such attempts is to obtain the external or internal shape (or geometry) of the object. However, among the attempts, the tested samples are always flat or in constant gradients. This means that the conclusions made have many limitations. Alternatively, quantitative evaluation of material thickness has also been done [15, 18, 19].

Samples of different thickness are produced and measured by LIT. The information is then stored into a look-up-table. Data in the look-up-table can be used inversely when evaluating other samples. However, the data measured using this technique is largely dependent on the surrounding factors. Once the surrounding factors change, the data stored are of less accuracy.

Hence, in this project, we will be discussing about two techniques in order to map the thickness of an object to the signal obtained from LIT while not affected by the shape of the object. In the first technique, we try to establish a universal function between the response signal and the thickness of the objects. This will allow the technique to calculate the thickness of samples directly from the signal obtained from LIT by inverting the function, even though the thickness may be varying along the surface. On the other hand, the second technique is an improved quantitative technique to let the computer to generate a sparse database from the signal obtained from samples and decide the thickness of the tested object from the class it belongs to inside the database. We also make an evaluation of both techniques by applying them onto real experiment data to see whether the techniques are applicable and accurate in deriving thickness of objects in real life. Besides, we also investigate the strength and weakness of stochastic gradient descent as a technique to generate the geometry of an object in real time.

2. Materials and Methods

2.1 Preparation of tested samples

In order to ensure that the results are not subject to the own shape of objects, we used FreeCAD to design 14 samples with different shapes. Figure 1 shows the shape of one sample.

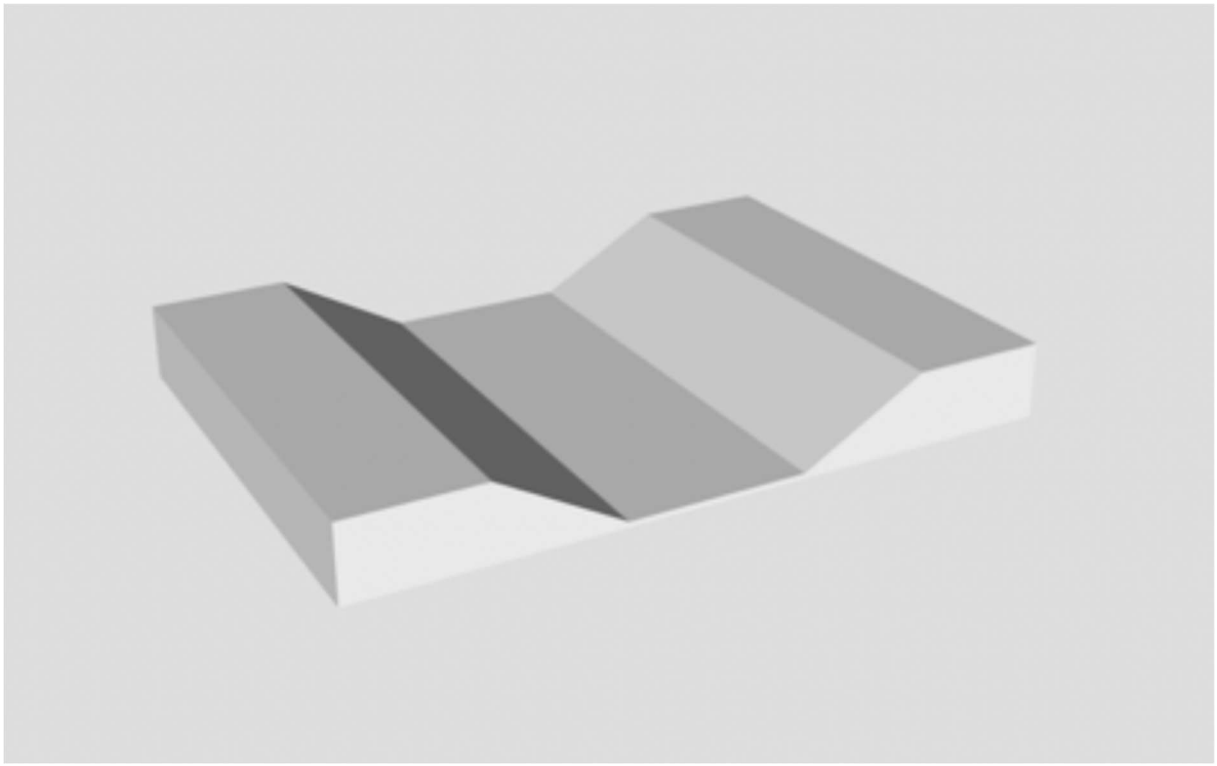

Figure 1: Designed model of one of the samples

Thickness of the samples varies along the surface, either quadratic (Figure 2a) or linear (Figure 2b).

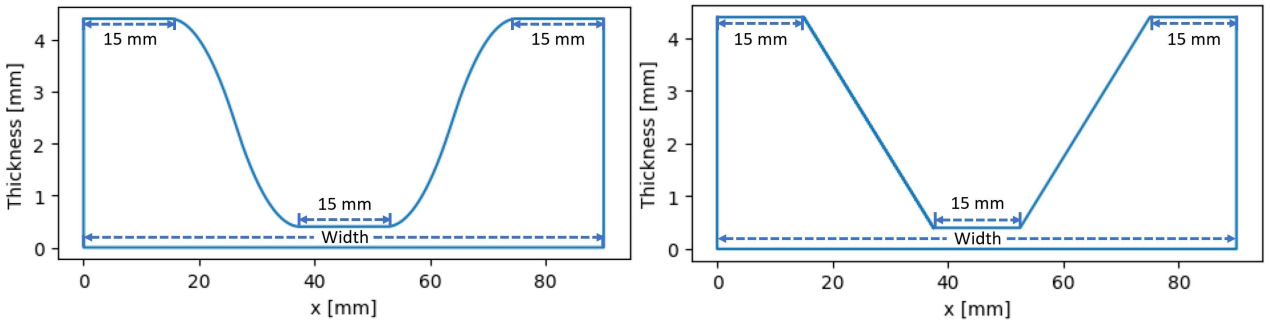

(a) Cross section of a curved sample

(b) Cross section of a linear sample

Figure 2: Different design of samples

Table 1 below shows the details of the samples used in the experiments.

Sample	Gradient type	Width [mm]	Min. Thickness [mm]	Max. Thickness [mm]
1	quadratic	90.0	0.4	4.4
2	quadratic	105.0	0.4	4.4
3	quadratic	75.0	0.4	4.4
4	quadratic	80.0	0.4	4.4
5	quadratic	85.0	0.4	4.4
6	linear	90.0	0.4	4.4
7	linear	105.0	0.4	4.4
8	linear	75.0	0.4	4.4
9	linear	80.0	0.4	4.4
10	linear	85.0	0.4	4.4
11	linear	60.0	0.4	4.4
12	linear	65.0	0.4	4.4
13	linear	70.0	0.4	4.4
14	linear	75.0	0.4	8.4

Table 1: Geometry of each sample used. Each sample has a height of 56 mm.

The samples were then printed out using Acrylonitrile Butadiene Styrene (ABS) in a 3D-printing machine. ABS is a kind of material that is widely used in 3D-printing for its many advantages [20].

2.2 Conduct of LIT experiments

In an LIT experiment, a schematic of the setup is shown in Figure 3.

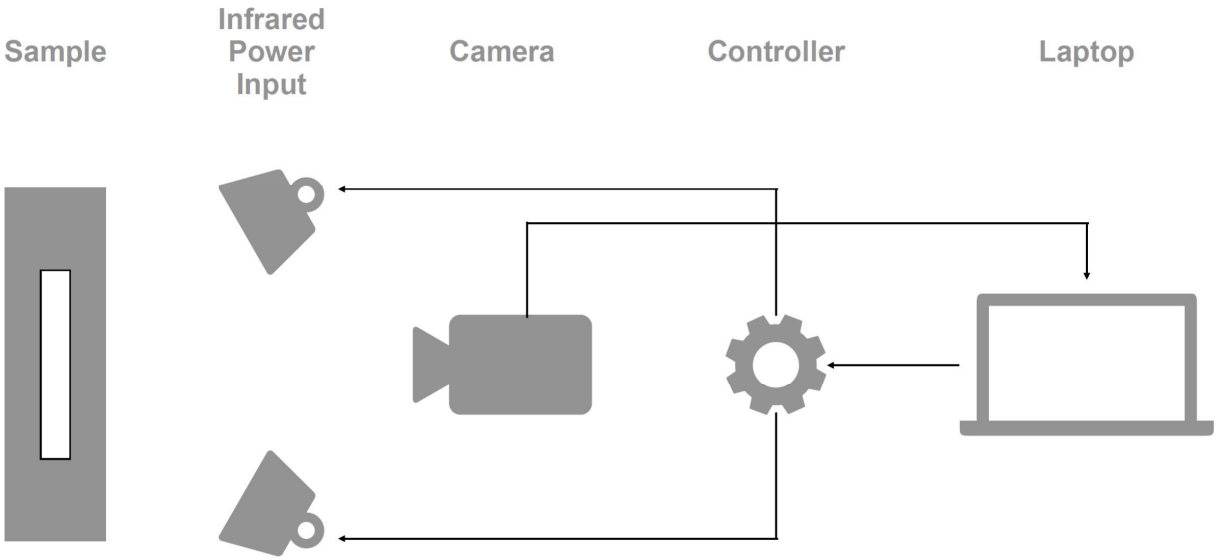

Figure 3: A schematic of the LIT experiment setup

Samples were heated by a pair of halogen lamps with a lock-in frequency of 0.01 Hz. A controller controlled by a laptop was used to control the halogen lamps so that they could heat periodically. The response image signals were captured by an infrared camera of 320 × 240 pixels and transmitted to the laptop for further processing. Each sample was heated over a period of 200 seconds at a lock-in frequency of 0.01 Hz and the images were captured in the speed of 1 frame per second so that 201 frames were captured in total for each sample.

2.3 Data processing

After the raw data of the data points at the pixels were acquired, lock-in calculations are applied in order to obtain the amplitude and phase signals, which are two common useful parameters in lock-in studies [21, 22]. The processing equations come from those of Bauer et al [23] as follows:

$$S_0(r,c) = \sum_{t=0}^{T}\left(I_t(r,c) \cdot \sin(2\pi ft)\right) \quad (1)$$

$$S_{-90}(r,c) = -\sum_{t=0}^{T}\left(I_t(r,c) \cdot \cos(2\pi ft)\right) \quad (2)$$

$$A = \sqrt{S_0^2 + S_{-90}^2} \quad (3)$$

$$\phi = \arctan\left(\frac{-S_{-90}}{S_0}\right) \quad (4)$$

where $S_0(r,c)$ is the in-phase signal at the pixel in row r and column c, $S_{-90}(r,c)$ is the out-of-phase signal at the pixel in row r and column c, t is the time, T is the total time, $I_t(r,c)$ is the response signal captured at the pixel in row r and column c, f is the lock-in frequency, A is the lock-in amplitude, and ϕ is the lock-in phase.

By plotting the graph of signal against time at each data points, we noticed that all the graphs plotted are similar. Figure 4 shows a typical graph of signal against time.

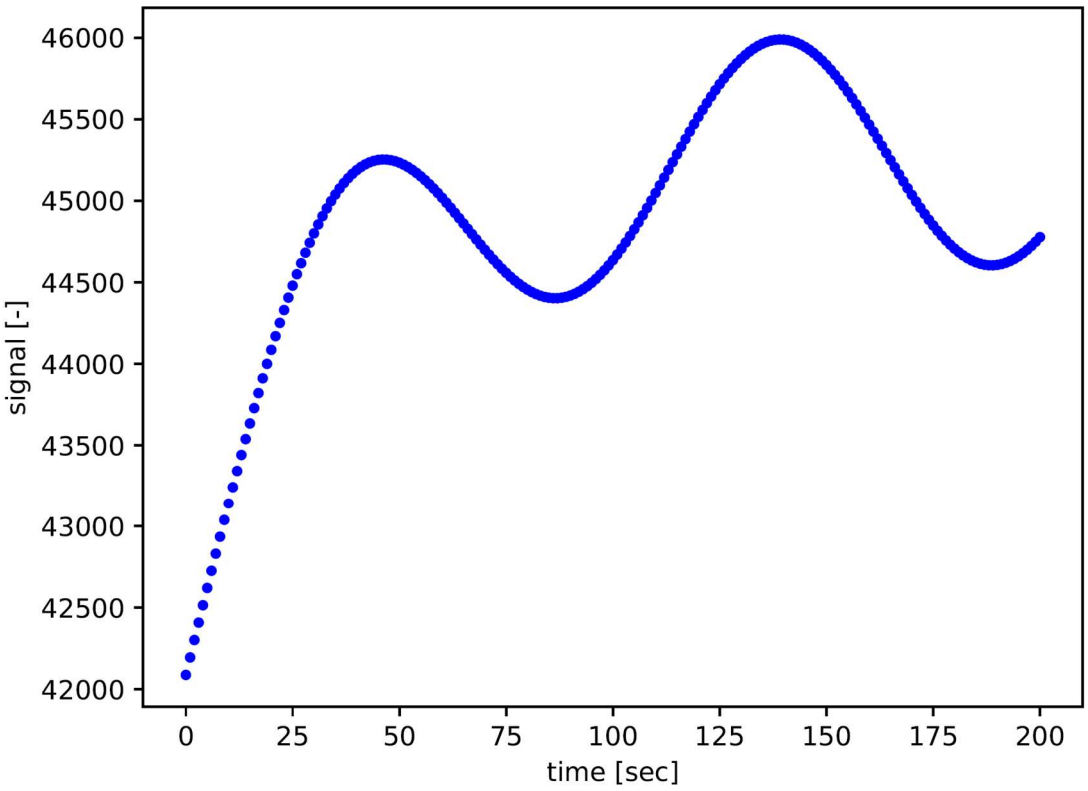

Figure 4: Graph of signal [-] against time [sec] at one data point

Other than the lock-in amplitude and phase, a set of other parameters were also derived from the raw data to pinpoint the thickness of the sample at every point more accurately. All these parameters were stored for every relevant image pixel on the samples for each measurement, and subsequently used to generate datasets. Purpose written algorithms were then created to identify the geometries of the samples.

3. Results and Discussion

From the raw experiment data, we have derived the lock-in phase, amplitude and also a set of other parameters for each data point of each sample. In order to map the thickness of an object to these parameters, we proposed two techniques.

3.1 Technique 1 – Deducing a universal function

Despite that currently there is no theoretical function that relates the lock-in phase, amplitude or other parameters to the thickness, we are able to fit the relationship to known functions by observing the trend [24]. Hence, the first technique that we discuss is to deduce a universal function that relates the lock-in phase, amplitude or other parameters to the thickness. If there is such a function, once we apply LIT onto an object and get the response signal, we can substitute the data into the universal function and hence directly calculate the thickness. In order to derive the relationship between thickness and all the parameters, we plotted graphs of every parameter against each other, and found that one of the parameters have a clear trend. We named this parameter “X Factor”. We also calculated the mean value of each parameters at each value of thickness to find a general trend.

When we plotted the graphs of phase against X Factor at each value of thickness ranging from 0.6 mm to 4.0 mm (Figure 5), we found that the graph at each value of thickness could respectively be fitted to a straight line (which is also plotted in Figure 5) and the gradients of the lines are about the same.

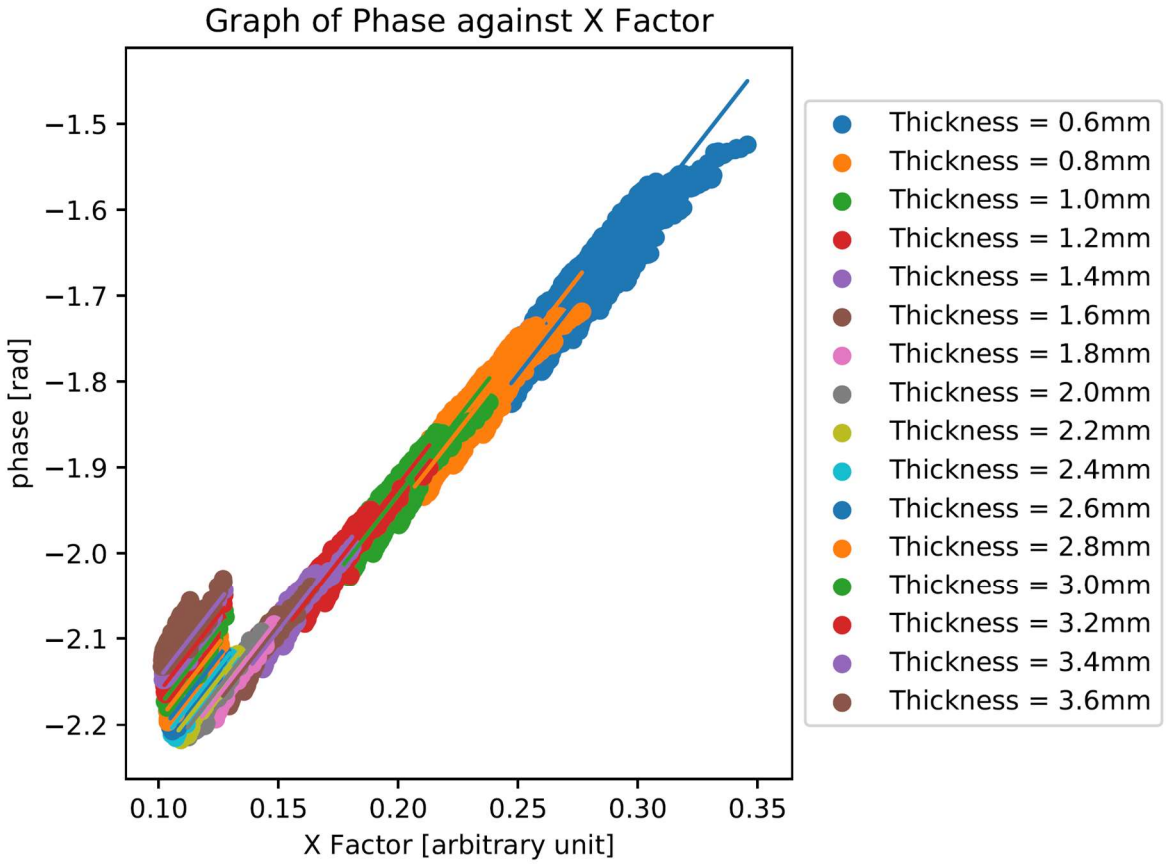

Figure 5: Graph of phase [rad] against X Factor [arbitrary unit] at different thickness

We knew that the expression of a straight line is $y = mx + c$. Hence, we predicted that the function linking phase, X Factor and thickness could be expressed as follows:

$$\phi = m \cdot X + c(\delta) \tag{5}$$

where ϕ is the phase, m is the common gradient, X is the X Factor (one of the parameters) as mentioned, δ is the thickness, $c(\delta)$ is a function of δ (i.e. thickness) that represents the y-intercept of each straight line. Therefore, the next step is to find the value of m and the expression of $c(\delta)$.

As the lines at different values of thickness share a similar gradient, we took the average of them as the value of m. To find the expression of $c(\delta)$, we plotted the graph of $c(\delta)$ against δ (Figure 6a) but there seemed to be no clear relationship. However, when we plotted the graph of $\overline{\phi}$, the mean phase value, against thickness on the same figure (Figure 6b), we noticed that the disparity between $\overline{\phi}$ and $c(\delta)$ gradually decreases and finally becomes constant at a certain value.

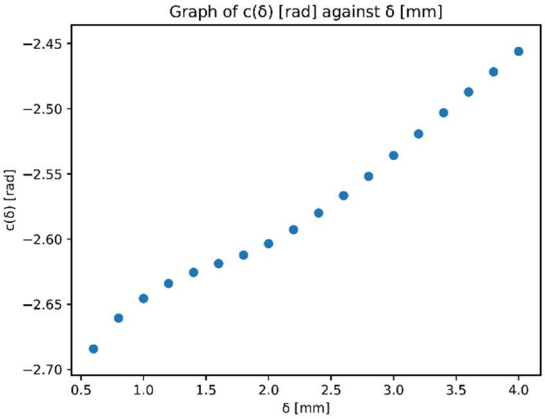

(a) Graph of $c(\delta)$ [rad] against δ [mm]

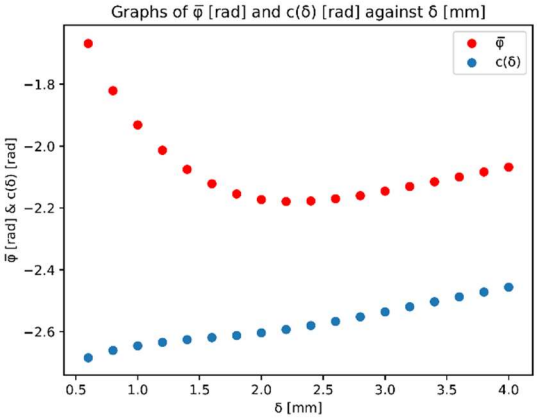

(b) Graphs of $c(\delta)$ [rad] and $\overline{\phi}$ [rad] against δ [mm]

Figure 6: Graphs used to deduce $c(\delta)$

Therefore, we plotted the graph of $\overline{\phi} - c(\delta)$ against δ (Figure 7a) and found that the curve could be fitted into an exponential function (Equation 6):

$$\overline{\phi} - c(\delta) = g(\delta) \tag{6}$$

where $g(\delta)$ here is an exponential function of δ.

As we have obtained the expression of $\overline{\phi} - c(\delta)$ and we wanted the expression of $c(\delta)$, we plotted the graph of $\overline{\phi}$ against δ (Figure 7b) to find the expression of $\overline{\phi}$. The curve could be fitted to a polynomial function (Equation 7):

$$\overline{\phi} = f(\delta) \tag{7}$$

where $f(\delta)$ here is a polynomial function of δ.

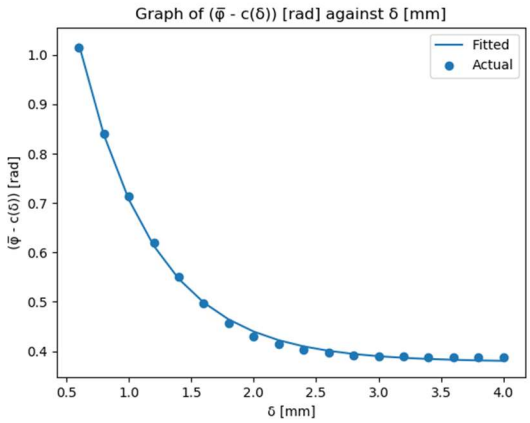

(a) Graph of $\overline{\phi} - c(\delta)$ [rad] against δ [mm]

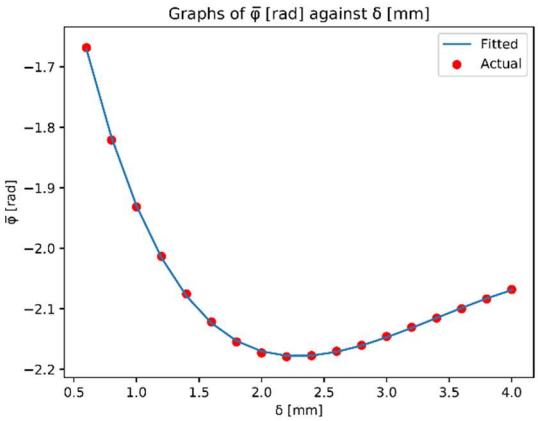

(b) Graphs of $\overline{\phi}$ [rad] against δ [mm]

Figure 7: Terms in the equation have an exponential and a polynomial relationship with δ

Now, Equation 5 could be rewritten in the following forms:

$$\phi = \mathrm{m} \cdot X + \mathrm{f}(\delta) - \mathrm{g}(\delta) \tag{8}$$

where all terms in the equation have been defined above. Before further application of Equation 8, we tested Equation 8 by substituting in the value of the variables except ϕ to get the fitted value of ϕ. We then compared the fitted value of ϕ with the actual value of ϕ by plotting the fitted value of ϕ against the actual value of ϕ and checking whether the scatter lies on the line $\mathrm{y} = \mathrm{x}$. We did so for each sample and all the graphs look similar to Figure 8.

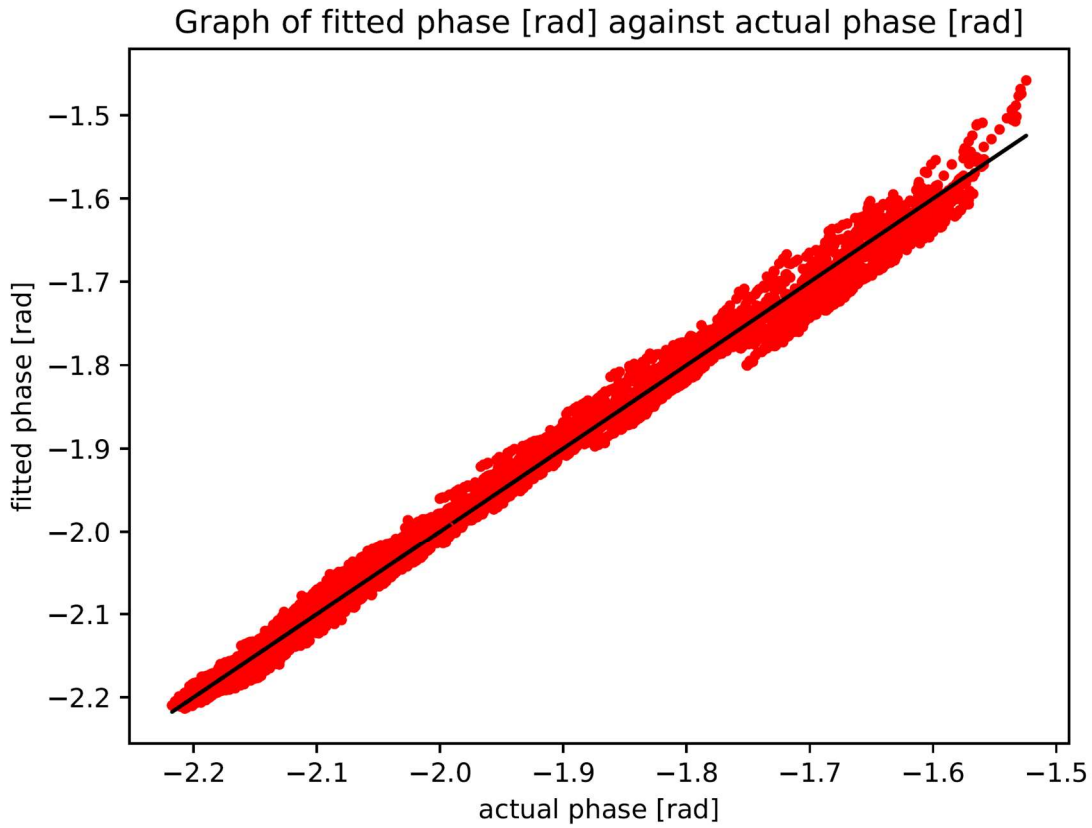

Figure 8: Graph of fitted phase [rad] against actual phase [rad]

From Figure 8 we can see that all the points lie around the line $\mathrm{y} = \mathrm{x}$ (the straight line in the figure), which means that the equation works. We then rewrote the equation in the following expression:

$$f(\delta) - g(\delta) = \phi - m \cdot X \tag{9}$$

As the value and/or expression of f, g, ϕ, m and X Factor in Equation 9 can all be obtained from the measurements, by inverting the function, it is possible to calculate the thickness. In other words, simply, δ is the solution of Equation 9.

3.2 Evaluation of Technique 1

Now that the linking function has been deduced, it is important to examine its applicability and success rate. We used several methods in evaluating this technique.

Just like what we have done to Equation 8, we substituted in the value of all the variables except the thickness to Equation 9. By solving Equation 9, we got the fitted value of thickness. We then compared the fitted value of thickness with the actual value of thickness in Figure 9.

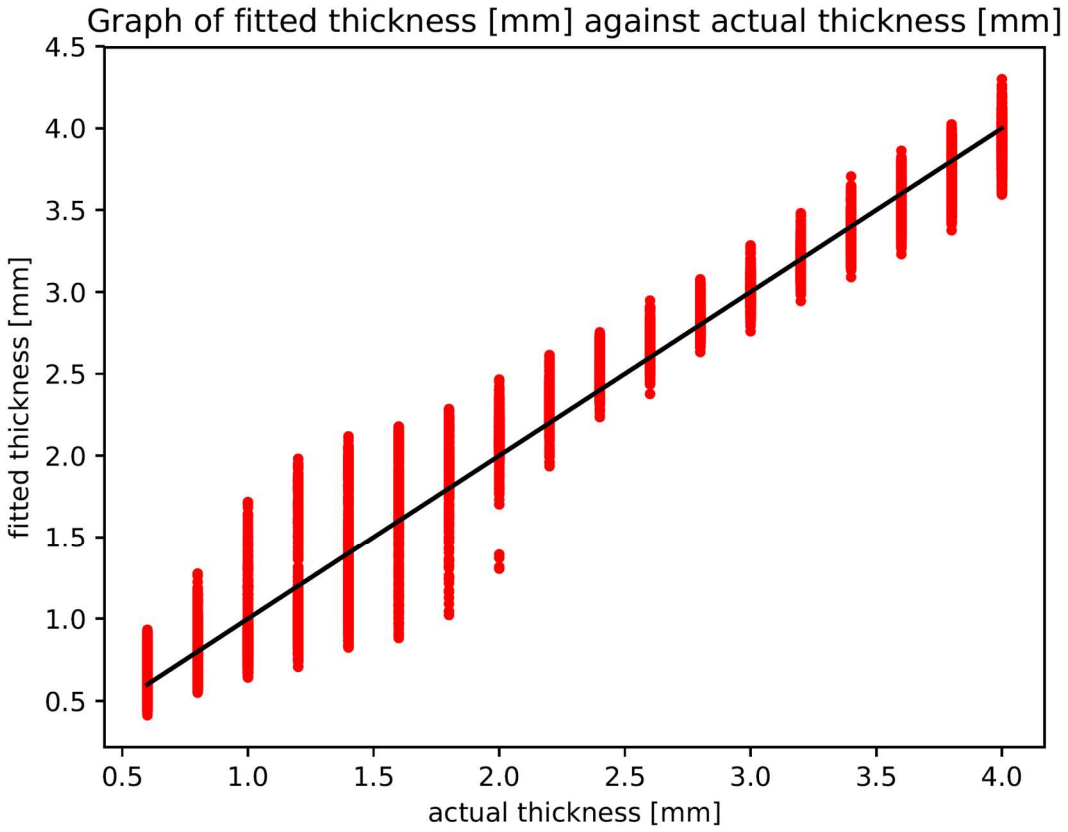

Figure 9: Graph of fitted thickness [mm] against actual thickness [mm]

We noticed that there are outliers that affect the result, but most fitted point is within a tolerance of 0.5 mm. Table 2 shows the percentage of points of which the fitted thickness has a tolerance of 0.5 mm of each sample. The data points at the edge of the samples have been filtered out because the existence of boundary effect [25], where the response signal from the edge will encounter more noises and hence perform irregularly [26]. Samples with a bad result are highlighted in red.

Sample	Percentage	Sample	Percentage	Sample	Percentage	Sample	Percentage
1	97.6	5	94.2	9	84.6	13	83.7
2	88.1	6	95.9	10	97.1	14	64.2
3	76.2	7	97.1	11	37.4		
4	93.2	8	67.5	12	68.7		

Table 2: Percentage of fitted thickness of which the tolerance is 0.5 mm

In order to determine whether the remaining outliers will badly affect the applicability of this technique, we did a 3D plot to check to result again. Here we take Sample 8 as an example (Figure 10).

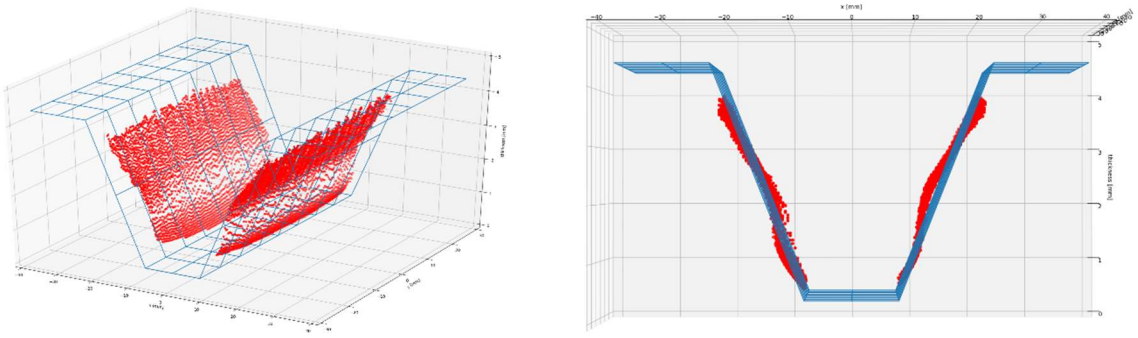

Figure 10: Fitted shape and actual shape of Sample 8

In Figure 10, the blue frame represents the actual shape and the red points represent the fitted shape. As we can see, a rough shape of the sample is fitted through this technique.

Root-mean-square deviation (RMSD) was also used to evaluate the technique due to its simplicity in comparing multi-dimensional data [27]. We used the dataset of one sample to derive the function (i.e. use the sample to train the function), applied it onto the dataset of another sample (use the sample to test the function), and calculated the RMSD between the fitted thickness and actual thickness, in order to find out what the reason is for some fit to be bad. Table 3 shows the results. Those with a high RMSD value are highlighted in red. We found that this technique might not perform well if the gradients of the training sample and testing sample differ by much.

Train \ Test	1	2	3	4	5	6	7	8	9	10	11	12	13	14
1	0.29	0.26	0.22	0.16	0.16	0.15	0.13	0.37	0.30	0.17	0.45	0.46	0.25	0.32
2	0.87	1.06	0.80	0.92	0.89	0.95	0.99	0.98	0.93	0.91	0.81	0.89	0.68	0.85
3	0.36	0.28	0.34	0.12	0.27	0.21	0.22	0.18	0.20	0.22	0.15	0.16	0.28	0.12
4	0.77	0.39	0.79	0.31	0.60	0.18	0.16	0.33	0.17	0.26	0.19	0.13	0.34	0.19
5	0.62	0.39	0.64	0.18	0.46	0.16	0.16	0.45	0.34	0.19	0.50	0.49	0.31	0.35
6	0.36	0.30	0.36	0.17	0.20	0.16	0.17	0.32	0.18	0.15	0.36	0.31	0.21	0.26
7	0.41	0.38	0.36	0.28	0.25	0.26	0.22	0.41	0.39	0.25	0.48	0.50	0.34	0.39
8	0.45	0.32	0.48	0.15	0.34	0.18	0.17	0.14	0.19	0.17	0.22	0.12	0.23	0.21
9	0.58	0.35	0.61	0.25	0.46	0.13	0.14	0.21	0.13	0.21	0.33	0.14	0.28	0.28
10	0.50	0.55	0.40	0.45	0.42	0.48	0.42	0.52	0.55	0.41	0.56	0.62	0.46	0.50
11	1.11	0.93	1.20	1.03	1.08	0.70	0.78	0.68	0.50	0.76	0.13	0.41	0.71	0.62
12	1.02	0.58	1.00	0.59	0.86	0.44	0.46	0.61	0.36	0.51	0.39	0.32	0.52	0.42
13	0.33	0.30	0.37	0.19	0.19	0.14	0.16	0.29	0.15	0.15	0.31	0.21	0.17	0.27
14	0.77	0.44	0.84	0.47	0.65	0.30	0.29	0.34	0.27	0.36	0.16	0.22	0.41	0.17

Table 3: RMSD value (rounded to 2 decimal places) of fitted thickness from actual thickness

3.3 Technique 2 – Generating a database

The second technique that we discuss is to generate a sparse database from the measurement and use the database to map thickness. Each sparse data point in the database contains the relevant parameters and if the parameters of a tested data point (except thickness, as it is still unknown) match one sparse data point, we predict the thickness of the tested data point according to the thickness of the sparse data point. Before generating the sparse database, we make an evaluation of the set of parameters to examine which parameters are relatively more critical by comparing the multi-dimensional distance. We find that 3 of them are critical compared with others. Hence, we only include the thickness, lock-in phase, amplitude, Parameter 1, Parameter 2 and Parameter 3 of each data point in the database we are going to generate.

From the dataset that contains the heating parameters we need (thickness, lock-in phase, amplitude, Parameter 1, Parameter 2 and Parameter 3) of each data point, we gather the data points that have similar value of parameters into one group. To achieve this, we set a resolution for each parameter. If all the parameters of two data points are

closer than the set resolution in these 6 dimensions, we take the average of all the parameters of these two data points as a new sparse data point. Note that every data point used has an equal weight.

After going through this process iteratively to all the data points of all samples, we get a database that contains many sparse data points. These data points are used to recognise the thickness of a sample based on the 5 parameters (lock-in phase, amplitude, Parameter 1, Parameter 2 and Parameter 3).

In this technique, the choice of resolution is very important. A low resolution increases the speed of fitting the geometries, as more data points will be closer than the resolution and hence there will be fewer sparse datapoints. However, precisely because the resolution is low, it will lower the accuracy of the database in mapping thickness. On the other hand, a high resolution despite being more accurate takes more time to fit the geometries, which lowers the efficiency of the technique. Therefore, we are still looking for an optimal resolution that achieve a balance between accuracy and efficiency. Currently the best resolution we have found is $(0.2,50,0.01,0.001,50,0.01)$ for (thickness, lock-in phase, amplitude, Parameter 1, Parameter 2 and Parameter 3).

3.4 Evaluation of Technique 2

Just like evaluation of Technique 1, we calculated the success rate of Technique 2 for each sample and we found that even with a very small tolerance (like 0.2 mm), the technique still performs well. Table 4 below shows the success rate of Technique 2 for each sample under different tolerances.

Sample	0.2 mm tolerance	0.5 mm tolerance	1.0 mm tolerance	1.5 mm tolerance
1	87.35	95.92	98.36	99.28
2	85.93	96.13	98.66	99.41
3	86.05	96.68	99.00	99.54
4	90.54	97.95	99.31	99.58
5	87.75	96.70	99.05	99.59
6	84.83	95.76	99.33	99.81
7	81.67	92.81	98.25	99.26
8	80.94	93.18	98.49	99.53
9	86.38	95.41	99.11	99.71
10	84.72	95.23	98.66	99.38
11	77.51	90.78	98.97	99.87
12	86.36	95.23	98.08	99.04
13	84.34	92.62	97.46	98.59
14	53.78	70.00	83.54	89.51

Table 4: Success rate (percentage) for each sample under different tolerances

In Table 4, samples with a relatively bad fit are highlighted in red. From Table 4 we can see that the success rate of Technique 2 is very high, even under a smaller tolerance than Technique 1. Therefore, this technique might be a more applicable idea in mapping geometries using LIT.

3.5 Using stochastic gradient descent (SGD) to identify geometries in real time

Now that we have found a technique that can identify geometries, we notice that the accuracy of the parameters is very important. If we do not get enough frames, the process of deriving parameters from the raw data will be of less accuracy and hence the parameters will be inaccurate. We noticed that in experiments we heated the samples over a period of 200 seconds in order to get 201 frames, but we do not know how many frames we actually need when it comes to actual application. Hence, we also investigated the use of stochastic gradient descent (SGD) in order to update the best-fit curve simultaneously during the measurement and hence get the geometry generated at the back end of the measurement.

Gradient descent is a popular iterative optimisation method [28, 29, 30] to find the minimum of loss functions which represents how close the fitted data are from the actual data. We started from an initial guess of the parameters, and then iteratively moved in the direction of the negative gradient at the current point. Mathematically, the iterative process can be expressed as equation 10:

$$x_{n+1} = x_n - \gamma_n \Delta F(x_n) \tag{10}$$

where x_n represents the fitted parameters in the nth iteration, γ_n is the step size, and $\Delta F(x_n)$ is the gradient.

Out of all kinds of gradient descent, stochastic gradient descent is one that run through every single set of data in the dataset [31, 32]. Based on this characteristic, whenever we get a new frame, we can use the new set of data to update the parameters and finally reach the set of parameters that lead to a minimum value of the loss function.

However, during the actual test of this method, we found that one significant drawback of stochastic gradient descent is that the value always converges to the local minimum points instead of the desired global minimum point. Hence, it is important to set the initial guess close enough to the global minimum point (i.e. in this case, the actual value of the parameters). Even though it is possible to use stochastic gradient descent to generate the thickness in real time, the time required to benchmark such a technique is significant. It will be interesting to derive a reliable method to obtain the geometry of samples in real time in future work.

4. Conclusion

This paper has shown the potential of two techniques in identifying the geometry of objects. When mapping thickness, despite that both techniques show a high success rate when given a tolerance, Technique 2 - generating a sparse database - performs better, which gives a good result even with a tolerance of 0.2 mm. Both techniques show that a relationship between the thickness at each data point and the response signal can be drawn. With such techniques, the function of LIT will be extended from identifying 2D shapes and temperature to identifying the 3D configuration of objects. The paper has also discussed the purpose and availability of using stochastic gradient descent in fitting the curve. Further studies can be conducted on making an initial guess close enough in order to get the geometry generated safely as LIT goes in real time. Further studies on LIT may also lead to new techniques that perform more stably and safely in identifying geometries or more purposes.

Acknowledgement

I would like to give special thanks to Dr Henry Goh Kok Hin from A*STAR for his time and guidance through this project.

References

[1] M. F. Modest, Radiative Heat Transfer. Academic Press, 2013.

[2] A. Kylili, P. A. Fokaides, P. Christou, and S. A. Kalogirou, "Infrared thermography (irt) applications for building diagnostics: A review," Applied Energy, vol. 134, pp. 531–549, 12 2014.

[3] Y. R. Montanholi, N. E. Odongo, K. C. Swanson, F. S. Schenkel, B. W. McBride, and S. P. Miller, "Application of infrared thermography as an indicator of heat and methane production and its use in the study of skin temperature in response to physiological events in dairy cattle," Journal of Thermal Biology, vol. 33, no. 8, pp. 468–475, 2008.

[4] I. Baroň, D. Bečkovský, and L. Míča, "Application of infrared thermography for mapping open fractures in deep-seated rockslides and unstable cliffs," Landslides, vol. 11, no. 1, pp. 15–27, 2012.

[5] R. Usamentiaga, P. Venegas, J. Guerediaga, L. Vega, J. Molleda, and F. G. Bulnes, "Infrared thermography for temperature measurement and non-destructive testing," Sensors, vol. 14, no. 7, pp. 12305–12348, 2014.

[6] D. Wu, T. Zweschper, A. Salerno, and G. Busse, "Lock-in thermography for nondestructive evaluation of aerospace structures," NDT.net, vol. 3, no. 9, 1998.

[7] T. Inagaki, T. Ishii, and T. Iwamoto, "On the ndt and e for the diagnosis of defects using infrared thermography," NDT & E International, vol. 32, no. 5, pp. 247–257, 1999.

[8] N. P. Avdelidis and A. Moropoulou, "Applications of infrared thermography for the investigation of historic structures," Journal of Cultural Heritage, vol. 5, no. 1, pp. 119–127, 2004.

[9] B. Lahiri, S. Bagavathiappan, P. Reshmi, J. Philip, T. Jayakumar, and B. Raj, "Quantification of defects in composites and rubber materials using active thermography," Infrared Physics & Technology, vol. 55, no. 2-3, pp. 191–199, 2012.

[10] P. Meinlschmidt and J. Aderhold, "Thermographic inspection of rotor blades," ECNDT, 2006.

[11] M. Svantner and Z. Veselý, "Active thermography for materials non-destructive testing," METAL 2014 - 23rd International Conference on Metallurgy and Materials, Conference Proceedings, pp. 851–856, 05 2014.

[12] T. Sakagami and S. Kubo, "Development of a new non-destructive testing technique for quantitative evaluations of delamination defects in concrete structures based on phase delay measurement using lock-in thermography," Infrared Physics & Technology, vol. 43, pp. 311–316, 06 2002.

[13] W. Bai and B. S. Wong, "Evaluation of defects in composite plates under convective environments using lock-in thermography," Measurement Science and Technology, vol. 12, no. 2, 2001.

[14] C. Meola, R. D. Maio, N. Roberti, and G. M. Carlomagno, "Application of infrared thermography and geophysical methods for defect detection in architectural structures," Engineering Failure Analysis, vol. 12, no. 6, pp. 875–892, 2005.

[15] C. Spiessberger, A. Dillenz, and T. Zweschper, "Active thermography for quantitative ndt of cfrp components," 2nd International Symposium on NDT in Aerospace 2010, pp. 1–7, 2010.

[16] J. Rantala, D. Wu, and G. Busse, "Amplitude-modulated lock-in vibrothermography for nde of polymers and composites," Research in Nondestructive Evaluation, vol. 7, no. 4, pp. 215–228, 1996.

[17] Z. Jin-Yu, M. Xiang-bin, and M. Yong-chao, “A new measurement method of coatings thickness based on lock-in thermography,” Infrared Physics & Technology, pp. 655–660, 2016.

[18] T. Sakagami, “Applications of pulse heating thermography and lock-in thermography to quantitative nondestructive evaluations,” Infrared Physics & Technology, vol. 43, no. 3-5, pp. 211–218, 2002.

[19] C. Wallbrink, S. Wade, and R. Jones, “The effect of size on the quantitative estimation of defect depth in steel structures using lock-in thermography,” Journal of Applied Physics, vol. 101, no. 10, 2007.

[20] Z. Weng, J. Wang, T. Senthil, and L. Wu, “Mechanical and thermal properties of absmontmorillonite nanocomposites for fused deposition modeling 3d printing,” Materials & Design, vol. 102, pp. 276–283, 2016.

[21] S. Pickering and D. Almond, “Matched excitation energy comparison of the pulse and lock-in thermography nde techniques,” NDT & E International, vol. 41, no. 7, pp. 501–509, 2008.

[22] T. Spirig, P. Seitz, O. Vietze, and F. Heitger, “The lock-in ccd-two-dimensional synchronous detection of light,” IEEE Journal of Quantum Electronics, vol. 31, no. 9, pp. 1705–1708, 1995.

[23] J. Bauer, O. Breitenstein, and J.-M. Wagner, “Lock-in thermography: A versatile tool for failure analysis of solar cells,” Electronic Device Failure Analysis, p. 6, 08 2009.

[24] H. Motulsky and A. Christopoulos, Fitting Models to Biological Data Using Linear and Nonlinear Regression: A Practical Guide to Curve Fitting. Oxford University Press, 2004.

[25] J. Rantala, D. Wu, A. Salerno, and G. Busse, “Lock-in thermography with mechanical loss angle heating at ultrasonic frequencies,” QIRT 96, pp. 389–393, 1996.

[26] S. Rainieri and G. Pagliarini, “Data filtering applied to infrared thermographic measurements intended for the estimation of local heat transfer coefficient,” Experimental Thermo and Fluid Science, vol. 26, no. 2-4, pp. 109–114, 2002.

[27] V. N. Maiorov and G. M. Crippen, “Significance of root-mean-square deviation in comparing threedimensional structures of globular proteins,” Journal of Molecular Biology, vol. 235, pp. 625–634, 05 1994.

[28] S. Madgwick, A. Harrison, and R. Vaidyanathan, “Estimation of imu and marg orientation using a gradient descent algorithm,” 2011 IEEE International Conference on Rehabilitation Robotics, 2011.

[29] A. Herschtal and B. Raskutti, “Optimising area under the roc curve using gradient descent,” Proceeding ICML ’04 Proceedings of the twenty-first international conference on Machine learning, p. 49, 2004.

[30] K. Fristen, “The free-energy principle: a rough guide to the brain?,” Trends in Cognitive Sciences, vol. 13, no. 7, pp. 293–301, 2009.

[31] S. Klein, J. P. W. Pluim, M. Staring, and M. A. Viergever, “Adaptive stochastic gradient descent optimisation for image registration,” International Journal of Computer Vision, vol. 81, 03 2009.

[32] W. Gardner, “Learning characteristics of stochastic-gradient-descent algorithms: A general study, analysis, and critique,” Signal Processing 6, pp. 113–133, 1984.